

# A<sup>2</sup>-Edit: Precise Reference-Guided Image Editing of Arbitrary Objects and Ambiguous Masks

Huayu Zheng<sup>1</sup> Guangzhao Li<sup>1,2</sup> Baixuan Zhao<sup>1</sup> Siqi Luo<sup>1</sup> Hantao Jiang<sup>1</sup>  
Guangtao Zhai<sup>1</sup> Xiaohong Liu<sup>1,2†</sup>

<sup>1</sup>Shanghai Jiao Tong University <sup>2</sup>Shanghai Innovation Institute

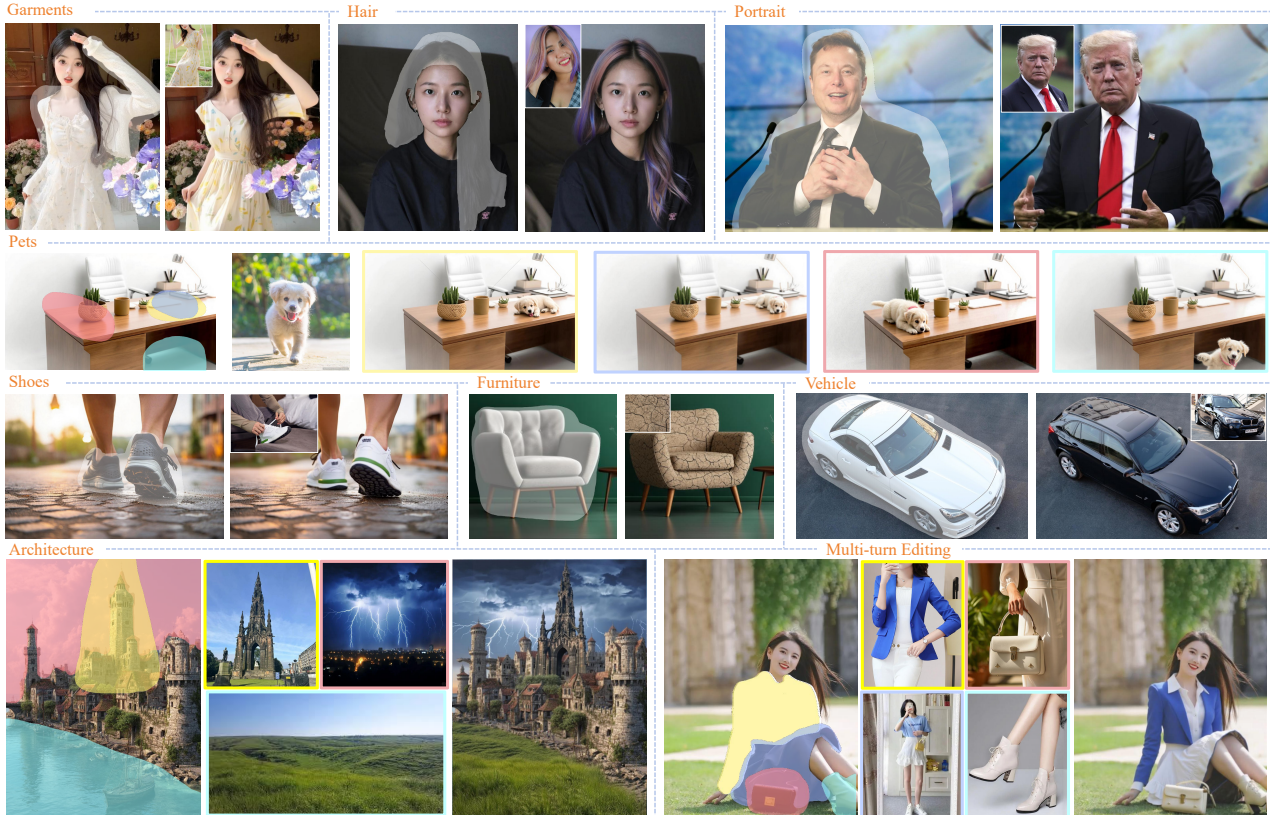


Figure 1. **Visual Results of A<sup>2</sup>-Edit:** A Unified Framework for Arbitrary-Object Inpainting. Our method supports a wide spectrum of real-world scenarios, delivering high-quality results across diverse object categories. The examples illustrate the generality and robustness of our method in handling various image editing tasks. More results are provided in the supplementary material.

## Abstract

We propose **A<sup>2</sup>-Edit**, a unified inpainting framework for arbitrary object categories, which allows users to replace any target region with a reference object using only a coarse mask. To address the issues of severe homogenization and limited category coverage in existing datasets, we construct a large-scale, multi-category dataset **UniEdit-500K**, which includes 8 major categories, 209 fine-grained subcategories, and a total of 500,104 image pairs. Such rich category diversity poses

new challenges for the model, requiring it to automatically learn semantic relationships and distinctions across categories. To this end, we introduce the **Mixture of Transformer** module, which performs differentiated modeling of various object categories through dynamic expert selection, and further enhances cross-category semantic transfer and generalization through collaboration among experts. In addition, we propose a **Mask Annealing Training Strategy (MATS)** that progressively relaxes mask precision during training, reducing the model’s reliance on accu-

<sup>†</sup>Corresponding author.

rate masks and improving robustness across diverse editing tasks. Extensive experiments on benchmarks such as VITON-HD and AnyInsertion demonstrate that A<sup>2</sup>-Edit consistently outperforms existing approaches across all metrics, providing a new and efficient solution for arbitrary object editing. Code and dataset will be released upon publication.

## 1. Introduction

In recent years, the rapid advancement of diffusion models (Ho et al., 2020; Peebles & Xie, 2023) has significantly propelled the progress of image generation technologies. However, effectively adapting these models to precise and controllable image editing tasks (Brooks et al., 2023; Zhang et al., 2023; Wang et al., 2024; Shen et al., 2024; Li et al., 2024; Xu et al., 2024b) remains challenging. Among various editing paradigms, reference-guided image inpainting has emerged as an important direction due to its strong controllability and practical value. This task requires transferring semantic content from a reference image to a masked target region while preserving object identity and maintaining natural consistency with the surrounding scene. Such capability forms the core technical foundation for applications including e-commerce product placement, virtual try-on, and personalized image customization.

Despite significant progress in recent years, existing reference-guided image inpainting methods still face critical bottlenecks in practical applications, which severely limit their generalization ability and usability. On the one hand, current approaches are typically optimized for specific object domains (e.g., garments (Chong et al., 2024; Xu et al., 2024a) or portraits (Parihar et al., 2024; Kulal et al., 2023)), while editing tasks across different categories exhibit fundamentally different modeling objectives. For instance, garment editing emphasizes texture consistency, portrait editing focuses on identity preservation and morphological variations, and rigid objects require accurate geometric and material representation. Such disparities in objectives make it difficult for a unified model to satisfy cross-category optimization requirements through a single processing pathway. However, most existing methods still employ shared parameter pathways to process inputs from all categories, lacking category-specific modeling mechanisms, which leads to significant cross-category performance degradation or even failure. Meanwhile, existing datasets exhibit highly homogeneous category distributions and limited coverage (He et al., 2024; Choi et al., 2021; Chen et al., 2024b;a; Song et al., 2025), further weakening the model’s ability to learn universal representations and exacerbating the generalization bottleneck.

On the other hand, current methods generally rely on high-precision segmentation masks to strictly define editing regions (Song et al., 2025; Chen et al., 2024b;a). In real-world scenarios, however, whether using user-drawn sketches or automatically generated detection boxes, achieving pixel-level accuracy is difficult. When mask quality deteriorates, model performance degrades significantly. Such reliance on idealized spatial guidance not only reduces interaction flexibility but also makes models fragile in open environments, thereby hindering their practical deployment and application.

To address the aforementioned challenges, we propose A<sup>2</sup>-Edit, a unified reference-guided image inpainting framework designed for Arbitrary object categories and Arbitrary levels of mask precision. A<sup>2</sup>-Edit enhances both cross-category generalization and mask robustness within a unified model architecture through dynamic expert modeling and a progressive training mechanism. Specifically, we introduce a **Mixture of Transformers (MoT)** architecture, which dynamically routes input features to specialized expert subnetworks based on the semantic characteristics and category attributes of the input object. This design enables category-specific modeling while facilitating cross-category knowledge collaboration, thereby significantly improving the generalization capability of the unified model. Meanwhile, we propose the **Mask Annealing Training Strategy (MATS)**, which progressively reduces mask precision during training. This strategy encourages the model to shift from relying on strict geometric boundaries toward developing stronger contextual semantic understanding and structural generation capabilities, thereby improving its adaptability to coarse masks.

To support the effective training of this unified framework and mitigate the issue of homogeneous data distribution, we further construct a large-scale multi-category dataset, **UniEdit-500K**. The dataset contains over **500,000** reference–target image pairs, covering **8 major categories** and **209 fine-grained subcategories**, spanning diverse object types including texture-dominant non-rigid objects and structure-dominant rigid objects. Such diversified object distribution provides critical support for collaborative modeling under heterogeneous editing objectives and enables strong cross-category generalization within a unified model.

In summary, our main contributions are:

- We propose A<sup>2</sup>-Edit, a highly generalized reference-guided image inpainting framework that breaks the constraints of domain-specific editing and rigid spatial guidance.
- We introduce a novel Mixture of Transformers (MoT) architecture and a Mask Annealing Training Strategy (MATS), enabling superior cross-category semantic

transfer and robust performance with arbitrarily imprecise masks.

- We construct UniEdit-500K, the most comprehensive dataset to date for this task, covering 8 major domains and 209 subcategories to support universal editing research. Extensive evaluations show that our approach achieves state-of-the-art performance across multiple datasets and objective metrics.

## 2. Related Works

### 2.1. Image Editing

Diffusion models have surpassed traditional generative models (VAEs, GANs) (Wang et al., 2020; Wu et al., 2019; Li et al., 2023; Liu et al., 2021; 2019; 2023) in image quality, establishing themselves as the mainstream choice for editing (Zhai et al., 2022; Maximov et al., 2020; Ramesh et al., 2022; Nichol et al., 2021; Shi et al., 2022). Early U-Net-based methods (Ho et al., 2020; Meng et al., 2021; Avrahami et al., 2022; Brooks et al., 2023; Xu et al., 2024a) often suffer from editing failures and detail distortions despite fine-grained masks. While Diffusion Transformers (DiTs) (Peebles & Xie, 2023; Esser et al., 2024; Labs, 2024a) have improved fidelity and controllability, recent text-driven approaches (IC-Edit (Zhang et al., 2025), DreamO (Mou et al., 2025), X2I (Ma et al., 2025), Qwen-Image (Wu et al., 2025)) still struggle with precise detail control. Mask-guided methods like Insert Anything (Song et al., 2025) and ACE++ (Mao et al., 2025) achieve strong performance on rigid objects, yet remain inadequate for non-rigid subjects (e.g., human faces, pets) due to complex deformations and identity sensitivity. We propose A<sup>2</sup>-Edit, a reference-based local editing framework that employs multi-precision mask fine-tuning to enable high-quality, fine-grained editing of diverse objects at arbitrary regions.

### 2.2. Universal Image Editing

Recent works have explored unified editing frameworks: ACE++ (Mao et al., 2025) unifies inputs via concatenated feature maps; Insert Anything expands training data across humans, objects, and garments; IC-Edit simulates in-context learning textually; UniReal (Chen et al., 2025) models editing as discontinuous video generation. However, these methods remain predominantly confined to rigid-object editing and struggle with non-rigid subjects requiring strong identity preservation. Text-driven approaches (Ma et al., 2025; Mou et al., 2025) fail to maintain subject identity, while mask-guided methods (Chen et al., 2024b;a; Mao et al., 2025; Parihar et al., 2024; He et al., 2024) are constrained by mask precision. We propose A<sup>2</sup>-Edit with a Mixture of Transformers (MoT) architecture that dynamically activates specialized experts based on semantic content and deforma-

tion characteristics, enabling a unified model that preserves structural stability for rigid objects and identity consistency for non-rigid subjects.

## 3. Method

### 3.1. Overview

The goal of image editing is to generate high-quality results in the target image by seamlessly integrating the subject from the reference image into the target scene, while adhering to the user-provided mask constraints and preserving the subject’s identity even when the mask is imprecise or rough. As illustrated in Figure 2, our method integrates two key components: (1) a Mixture-of-Transformers (MoT) editing module that dynamically routes input features to different expert networks for differentiated modeling of diverse objects (§3.2); and (2) a Mask Annealing Training Strategy (MATS) that gradually reduces mask precision to shift the model from relying on strict spatial constraints to developing stronger contextual understanding and content generation capabilities (§3.3). Working jointly, these components enable the model to handle complex, multi-category image editing tasks by maintaining fine-grained details and identity features of the reference element, while producing high-quality, naturally integrated results even under relaxed mask constraints.

### 3.2. Mixture of Transformers

Existing image editing methods typically adopt a unified parameter pathway to process inputs from different object categories. However, such a design struggles to accommodate diverse editing objectives and often exhibits poor generalization to unseen categories. In recent years, the *Mixture-of-Experts* (MoE) paradigm (Jacobs et al., 1991; Han et al., 2025; Dai et al., 2024) has been widely adopted in large-scale models, but sparse experts are typically introduced only in the FFN layers, while the Attention modules remain shared.

In image editing tasks, different object types require not only *category-specific content transformations* (handled by FFN), but also *specialized relational modeling* (handled by Attention), such as shape alignment, texture consistency, and spatial coherence. Therefore, applying expert modeling only to the FFN layers is often insufficient to capture these structural relationships. Meanwhile, recent studies (Yang et al., 2025; Jin et al., 2025) further show that Attention itself contains functionally decomposable subspaces and can benefit from conditional expert selection.

Based on these observations, we adopt a **Mixture-of-Transformers (MoT)** architecture that extends expert routing from the conventional FFN-only design to both the Attention and Feed-Forward Network (FFN) modules. Specif-

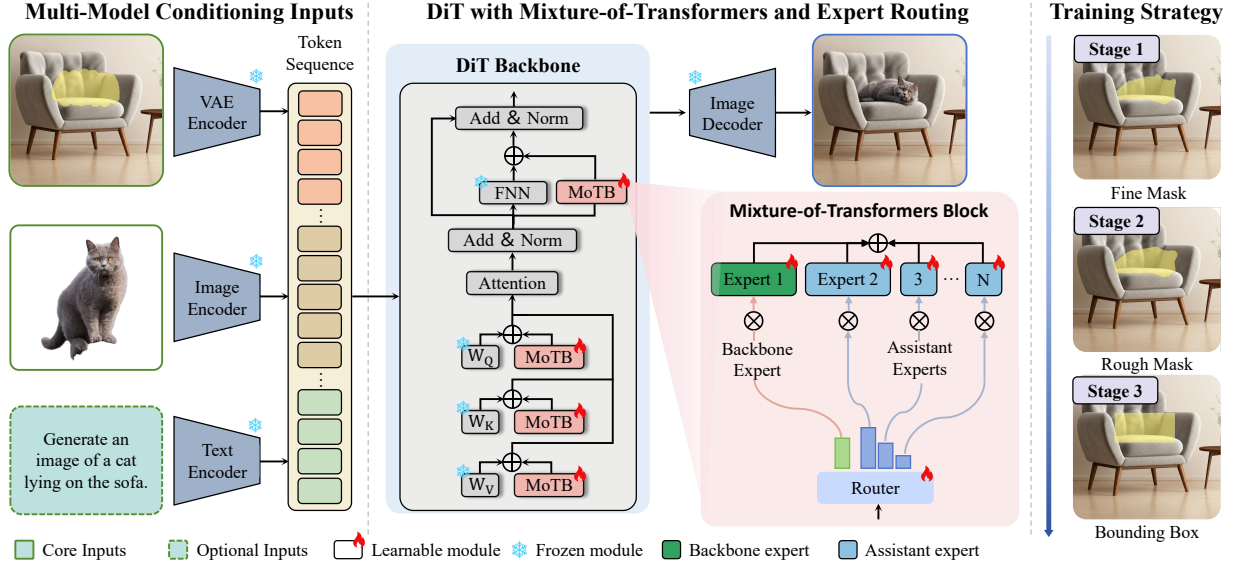


Figure 2. Overview of the A<sup>2</sup>-Edit framework. Our architecture takes a reference image, target image, and user mask as core inputs, encodes them into a unified feature space, and feeds the fused features into Mixture-of-Transformers (MoT) module. The MoT Block (MoTB) denotes an expert-specific Transformer block embedded within the attention and feed-forward layers. The model then dynamically routes features to specialized experts for differentiated modeling. Model is trained via Mask Annealing Training Strategy (MATS), a three-stage training process. Final outputs are decoded by a VAE decoder for high-fidelity results.

ically, we introduce **Mixture-of-Transformers Blocks (MoTB)** in each Transformer layer, where multiple expert adapters are conditionally activated through a routing mechanism, enabling category-aware parameter specialization. Each expert is implemented as a lightweight **LoRA adapter** (Hu et al., 2022), enabling efficient parameter specialization with minimal computational overhead.

### 3.2.1. MULTIMODAL FEATURE ENCODING.

Given a reference image  $I_r$ , a target image  $I_t$ , and a mask  $M$ , we first extract the foreground of the reference image to obtain a clean subject representation  $\tilde{I}_r$  (Chen et al., 2024b; Shin et al., 2024). The reference image is encoded to obtain visual features  $F_r$ , while the target image  $I_t$  with mask guidance is encoded into latent features  $F_t$ . If a text prompt  $P$  is provided, it is encoded into textual features  $F_p$ . All features are projected into a shared multimodal embedding space and fused into a unified token sequence:

$$\mathbf{x} = \text{Fuse}(F_t, F_r, F_p). \quad (1)$$

### 3.2.2. EXPERT ROUTING.

We employ a multilayer perceptron as the gating network  $G(\cdot)$  to predict routing weights over  $N$  experts. To balance model capacity and efficiency, we adopt an Anchor-Guided Routing (AGR) strategy  $\mathcal{T}_{AGR}(\cdot)$ . A backbone expert is always activated to provide universal knowledge, while assistant experts are activated only if their routing weights exceed the backbone’s weight (or the highest-weighted expert otherwise). The activated expert set is defined as  $\mathcal{S} = \mathcal{T}_{AGR}(\mathbf{w}(\mathbf{x}))$ .

### 3.2.3. MOT LAYER WITH LORA EXPERTS.

For each linear transformation  $W$  in the Transformer layer (e.g.,  $W_Q, W_K, W_V$  in attention and  $W_1, W_2$  in FFN), we use a shared backbone weight with expert-specific LoRA increments:

$$W = W^{(0)} + \sum_{i \in \mathcal{S}} w_i(\mathbf{x}) \Delta W_i, \quad \Delta W_i = A_i B_i. \quad (2)$$

where  $W^{(0)}$  denotes the shared backbone parameters and  $\Delta W_i$  represents the LoRA update of the  $i$ -th expert. Notably, routing is performed only once per layer, and the same routing weights are shared by both the Attention and FFN modules to ensure consistent modeling behavior.

### 3.2.4. TRAINING AND INFERENCE.

All routing parameters and LoRA experts are optimized jointly in an end-to-end manner. During training, routing gradients automatically encourage experts to specialize in different category patterns while preserving shared knowledge. During inference, only a small subset of experts (the backbone and a few assistant experts) are activated, enabling efficient sparse computation. For out-of-distribution inputs, the gating network selects suitable expert combinations according to feature similarity, improving generalization and robustness.

## 3.3. Mask Annealing Training Strategy

Many models overly rely on idealized inputs, limiting user interaction freedom and degrading performance with poor mask quality. We propose the Mask Annealing Training

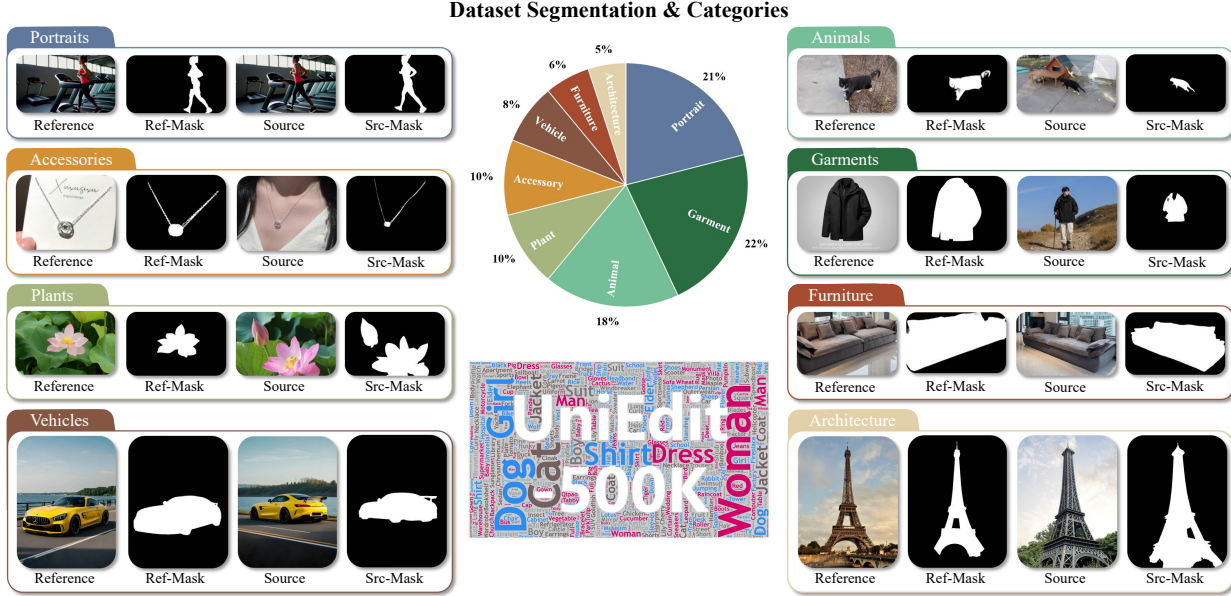


Figure 3. An overview of our UniEdit-500K dataset. The central pie chart illustrates the proportional distribution across the eight major categories. The word cloud below visualizes the diversity of object classes within the dataset. Surrounding the center are representative examples from each category (Portraits, Accessories, Plants, Vehicles, Animals, Garments, Furniture, and Architecture), showcasing the data format which includes a reference image, a source image, and their corresponding segmentation masks.

Strategy (MATS), which gradually reduces input mask precision to guide the model from relying on fine spatial constraints to stronger contextual reasoning and content generation—enabling adaptive adjustments across objects/scenarios. It includes three training stages: *Fine Mask Training*, *Augmented Rough Mask Training*, and *Bounding Box Training*.

**Fine Mask Training.** In the initial training stage, we use high-precision segmentation masks strictly aligned with the target object to indicate the editing region. The model is provided with the target image  $I_t$ , its high-precision mask  $M_t \in \{0, 1\}^{H \times W}$ , and reference image  $I_r$ .

**Augmented Rough Mask Training.** To reduce overreliance on mask boundaries and enhance tolerance for rough inputs, the second stage introduces mask augmentation. First, isotropic morphological dilation is applied to the fine mask  $M_t$ :

$$M_t^{dil} = M_t \oplus B_a, \quad (3)$$

where  $\oplus$  denotes dilation and  $B_a$  is a circular structuring element of radius  $a$ , simulating user-drawn edge extensions. The external contour set  $\mathcal{C} = \{\mathbf{p}_i = (x_i, y_i)\}_{i=1}^N$  is then extracted from  $M_t^{dil}$ . Contour points undergo spatially correlated random displacement via Perlin noise (Perlin, 1985) to emulate human drawing errors:

$$\Delta \mathbf{p}_i = \alpha \cdot \begin{bmatrix} \mathcal{N}(x_i \cdot s, y_i \cdot s) \\ \mathcal{N}((x_i + \delta) \cdot s, (y_i + \delta) \cdot s) \end{bmatrix}, \quad (4)$$

where  $\alpha$  controls displacement magnitude,  $s$  is noise scale, and  $\delta$  decouples axes. Disturbed points are:

$$\hat{\mathbf{p}}_i = \Pi_{\Omega}(\mathbf{p}_i + \Delta \mathbf{p}_i), \quad (5)$$

with  $\Pi_{\Omega}$  projecting coordinates to the image domain. The augmented rough mask  $\tilde{M}_t$  is derived from  $\hat{\mathcal{C}} = \{\hat{\mathbf{p}}_i\}$ .

**Bounding Box Training.** provided.

In the final stage, we further simplify the mask by extending the rough mask  $\tilde{M}_t$  to the target object’s bounding box  $\tilde{M}_t$ . Without fine shape priors, the model infers the object’s pose, scale, and local structure independently, generating reasonable, naturally integrated content with the reference image. This phase enhances creative generation capability and adaptability to objects (e.g., human faces, pets) with only rough localization.

## 4. UniEdit-500K

### 4.1. Comparison with Existing Datasets

Recent works have made remarkable progress in the field of image generation. However, most existing methods focus on single tasks, perform poorly on out-of-distribution object categories, struggling to adapt to complex and diverse real-world scenarios. We attribute this issue partly to the constrained categories in existing datasets: the FreeEdit (He et al., 2024) dataset mainly focuses on animals and plants, while the VITON-HD (Choi et al., 2021) dataset specializes in garments. Although AnyDoor (Chen et al., 2024b) and MimicBrush (Chen et al., 2024a) contain large scale data,

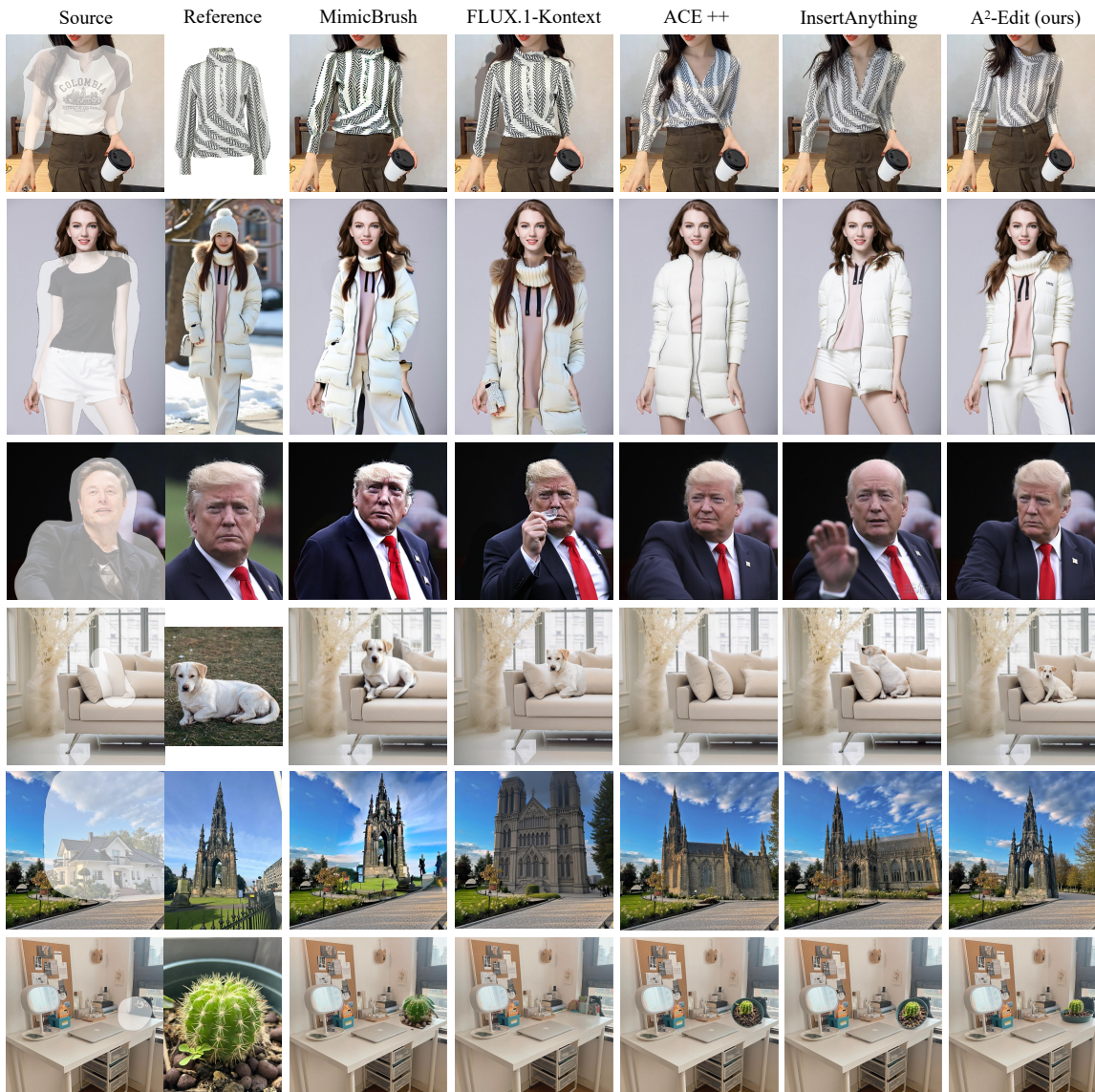


Figure 4. **Qualitative comparison with existing mask-guided image editing methods.** Our method consistently produces more coherent structures, sharper details, and better semantic alignment with the target edit compared to existing methods (MimicBrush (Chen et al., 2024a), FLUX.1-Kontext (Labs, 2025b), ACE++ (Mao et al., 2025) and InsertAnything (Song et al., 2025)).

they include very few samples related to human insertion. While AnyInsertion (Song et al., 2025) expands categories to include humans, objects, and garments, it still falls short in category coverage. To address these limitations, we construct UniEdit-500K, a large-scale dataset covering multiple domains and diverse object types. This dataset comprises eight major categories—garments, portraits, animals, plants, accessories, furniture, vehicles, and architecture—further refined into 209 fine-grained subcategories. The diversity of data categories enhances the model’s comprehensive capabilities across various object types. More importantly, such diversity provides the model with abundant examples to learn both distinctions and correlations among different categories, thereby establishing essential conditions for

achieving genuine generalization.

## 4.2. Data Construction

We employed a multi-strategy hybrid approach to jointly construct the large-scale UniEdit-500K dataset.

For **garments and accessories** categories, we build upon the VITON-HD and DressCode datasets, and additionally collect a large number of *person-wearing-item* scene images from open-licensed platforms such as Pixabay that allow research use and redistribution. Furthermore, we supplement the dataset with images sourced from community platforms under explicit creator permission. During data construction, we pair the standalone item images with their corresponding

wearing-scene images to form high-quality image pairs.

For **portraits and animals**, which requires strong identity consistency, we adopted a video-driven dynamic sampling method. The video data is sourced from the VidGen-1M dataset (Tan et al., 2024) (Apache License 2.0). Given a video and a specified subject category, we first performed frame sampling and used Grounding DINO (Liu et al., 2024) and Segment Anything Model (SAM) (Kirillov et al., 2023) to extract subject masks; then, we computed quality scores via no-reference image quality assessment to filter high-quality frames; finally, we selected the optimal two frames based on the degree of subject variation as the output.

For **plants, vehicles, architecture, and furniture** objects, we collected multi-view images from open data platforms, combining manual verification and automatic pairing strategies to construct image pairs with sufficient viewpoint variation.

In addition, we utilized NanoBanana to address missing data and balance the dataset for certain domains. After obtaining matched image pairs, we performed object detection using Grounding DINO with the obtained object category  $c$ , producing bounding boxes  $b_i$ . Then, based on  $b_i$ , we generated binary segmentation masks  $M_i \in \{0, 1\}^{H \times W}$  using the SAM. Ultimately, we obtained paired reference and target images along with their corresponding masks, as illustrated in Figure 3. For images obtained with creator authorization, we strictly restrict usage to the explicitly permitted subset to ensure compliance and proper data governance.

### 4.3. Dataset Overview

The UniEdit-500K dataset consists of a training subset and a test subset. The training set contains 500,104 samples covering eight major categories (clothing, portraits, animals, plants, accessories, furniture, vehicles, and buildings), comprising a total of 209 fine-grained subcategories. Each data sample includes a reference image, a target image, and the corresponding mask. The composition of the dataset is illustrated in Figure 3, with additional details provided in the supplementary materials. For evaluation, we constructed a test set of 200 image pairs, selecting 25 samples from each major category to comprehensively assess the model’s capability across different object classes.

## 5. Experiments

### 5.1. Experimental Setup and Configuration

**Implementation Details.** We adopt FLUX.1 Fill (Labs, 2024b) as the backbone of our approach, which is an open-source image inpainting model based on the DiT architecture. The encoder utilizes a T5 text encoder (Raffel et al.,

2020) and a SigLIP image encoder (Zhai et al., 2023). The model is configured with LoRA of rank 32, 8 expert sub-networks, and the Anchor-Guided Routing strategy—where one backbone expert is always activated, and assistant experts are activated based on routing weights. During training, the batch size is set to 8, and all images are processed at a resolution of 1024×1024. All experiments are conducted on a cluster of 4 NVIDIA A100 GPUs. We use our self-constructed UniEdit-500K dataset as the main training set and train the model for 6000 steps in total, including 3000 steps with fine masks, 1500 steps with augmented rough masks, and 1500 steps with bounding box masks. In terms of computational cost, during inference on a single NVIDIA A100 (80GB), our model reaches a peak memory usage of 42 GB (42,074 MiB), which is slightly higher than the 39,884 MiB required by the baseline model. For 50 sampling steps, the average inference time of our model is approximately 30 seconds, compared to about 32 seconds for the baseline model (both results are averaged over 100 evaluation samples).

**Evaluation Settings.** We evaluate our method on two standard datasets: VITON-HD (Choi et al., 2021) and AnyInsertion (Song et al., 2025). VITON-HD serves as the standard benchmark for virtual try-on and garment insertion tasks. The AnyInsertion test set contains 100 samples, including 40 object samples, 30 garment samples, and 30 portrait samples. In addition, to comprehensively validate cross-category generalization capability, we construct a test set of 200 samples by selecting 25 samples from each of the eight major categories in UniEdit-500K. For evaluation metrics, we adopt five quantitative measures: CLIP-I (Radford et al., 2021), DINO-I (Oquab et al., 2023), LPIPS, FID, and a VLM-based score. CLIP-I, DINO-I, and LPIPS are used to assess semantic alignment and perceptual similarity from multiple perspectives, while FID evaluates the overall distributional realism of the generated images. Moreover, since metrics such as CLIP, DINO, and LPIPS do not always adequately capture boundary artifacts, visual realism, and local consistency, we further introduce a Vision-Language Model (VLM)-based evaluation protocol. Specifically, we employ a large language model to score the generated results along three aspects: boundary quality, realism, and local consistency. The final VLM score is obtained by averaging these three dimensions across all samples. Detailed evaluation protocols and scoring prompts are provided in the supplementary material.

### 5.2. Quantitative Comparison

**Common Domain Evaluation.** In this study, we compare A<sup>2</sup>-Edit with FLUX.1-Fill-dev (Labs, 2024b), AnyDoor (Chen et al., 2024b), MimicBrush (Chen et al., 2024a), FLUX.1-Kontext-dev (Labs, 2025b), ACE++ (Mao et al., 2025) and InsertAnything (Song et al., 2025)) on the

Table 1. **Qualitative comparison with existing image editing methods.** Evaluations conducted on VTON-HD and AnyInsertion datasets show that our A<sup>2</sup>-Edit model significantly outperforms existing methods. The best and second-best results are demonstrated in **bold** and underlined, respectively. Note that higher DINO-I and CLIP-I scores indicate better performance, while lower LPIPS values are preferred.

Method	VTON-HD						AnyInsertion					
	Fine Mask			Rough Mask			Fine Mask			Rough Mask		
	DINO-I	CLIP-I	LPIPS									
FLUX.1-Fill	58.59	72.59	0.1241	46.18	69.04	0.1509	50.37	66.06	0.1962	43.57	62.89	0.2673
AnyDoor	59.18	72.54	0.1270	45.99	69.38	0.1587	48.15	65.01	0.2070	42.47	60.67	0.2854
MimicBrush	58.99	73.01	0.1022	49.13	68.54	0.1479	50.29	68.88	0.1878	47.89	65.13	0.2011
FLUX.1-Kontext	60.09	79.44	0.0800	56.11	77.91	0.0972	59.49	74.70	0.1094	54.15	74.05	0.1384
ACE++	<u>62.33</u>	78.00	0.0767	58.78	<u>78.33</u>	0.0813	57.69	74.33	0.1241	56.44	73.80	0.1327
Insert Anything	62.15	<u>79.96</u>	<u>0.0728</u>	<u>60.87</u>	78.22	<u>0.0809</u>	<u>60.90</u>	<u>76.11</u>	<u>0.0978</u>	<u>60.50</u>	<u>75.98</u>	<u>0.0992</u>
<b>A<sup>2</sup>-Edit (Ours)</b>	<b>64.07</b>	<b>81.53</b>	<b>0.0677</b>	<b>63.79</b>	<b>80.19</b>	<b>0.0685</b>	<b>61.67</b>	<b>77.45</b>	<b>0.0909</b>	<b>61.73</b>	<b>77.27</b>	<b>0.0903</b>

Table 2. **Quantitative comparison on the UniEdit test set across diverse object categories.**

Method	UniEdit									
	Fine Mask					Rough Mask				
	DINO-I ↑	CLIP-I ↑	LPIPS ↓	FID ↓	VLM ↑	DINO-I ↑	CLIP-I ↑	LPIPS ↓	FID ↓	VLM ↑
FLUX.1-Fill	45.61	63.69	0.2519	93.70	42.7	40.09	61.58	0.3739	128.91	26.3
AnyDoor	46.76	64.23	0.2534	92.19	41.0	40.42	61.39	0.3623	120.80	28.3
MimicBrush	50.02	68.56	0.2133	86.23	47.7	45.07	64.36	0.2871	100.54	36.3
FLUX.1-Kontext	53.47	73.99	0.1403	70.54	52.3	48.29	70.56	0.2091	80.94	54.0
ACE++	<u>58.13</u>	74.70	0.1164	62.30	76.0	<u>56.68</u>	<u>73.66</u>	<u>0.1219</u>	<u>63.19</u>	74.7
Insert Anything	56.22	<u>74.87</u>	<u>0.1121</u>	<u>59.99</u>	<u>78.7</u>	56.13	73.37	0.1243	61.48	<u>75.0</u>
<b>A<sup>2</sup>-Edit (Ours)</b>	<b>61.71</b>	<b>76.89</b>	<b>0.0898</b>	<b>57.72</b>	<b>82.3</b>	<b>62.28</b>	<b>77.45</b>	<b>0.0897</b>	<b>54.62</b>	<b>79.3</b>

VITON-HD and AnyInsertion datasets, using both fine and rough masks. The rough masks are obtained by applying isotropic morphological dilation to the fine masks. As shown in Table 1, A<sup>2</sup>-Edit achieves the best performance across all metrics, indicating that A<sup>2</sup>-Edit has the ability to perform as well as specialized models in common data domain. Additional qualitative comparisons with representative text-guided editing models, including Qwen-Image-Edit-2509 (Qwen, 2025) and FLUX.2-klein-4B (Labs, 2025a), are provided in the supplementary material for cross-paradigm comparison.

**Generalization Ability Evaluation.** To test the model’s ability in different object categories, we evaluate A<sup>2</sup>-Edit against other methods on the UniEdit test set. As presented in Table 2, A<sup>2</sup>-Edit significantly outperforms existing approaches on this multi-category dataset while maintaining comparable performance with those in common domains. This indicates that A<sup>2</sup>-Edit exhibits more stable performance and stronger generalization capability when dealing with diverse object categories in real-world scenarios, showcasing superior universality.

**User Study.** In Figure 6, we showcase the outcomes of the

results of our user study. A total of 24 participants were recruited to compare the images generated by our method with those produced by various baseline approaches. The reported percentages indicate the proportion of participants who preferred the results of a given model in each comparison. The result demonstrates that our method consistently receives higher preference from participants compared to all evaluation methods.

### 5.3. Qualitative Comparison

Figure 4 presents a comprehensive qualitative comparison between A<sup>2</sup>-Edit and MimicBrush, FLUX.1-Kontext, ACE++, and InsertAnything across a variety of inpainting-based image editing tasks, including garments, portraits, pets, and other object categories. All experiments are conducted using hand-drawn rough masks. In several challenging editing scenarios, MimicBrush shows clear limitations in preserving fine details and fails to maintain identity consistency in portrait editing. FLUX.1-Kontext exhibits instability when handling mask boundaries, often producing noticeable edge artifacts and visible seams. InsertAnything and ACE++ frequently struggle to correctly interpret editing



Figure 5. **Ablation Study.** Removing the framework, training data, or MATS reduces generation quality and cross-category generalization, while progressively adding each component significantly improves detail fidelity and the model’s ability to handle rough masks.

Table 3. **Ablation Result.** We evaluate model variants on UniEdit. w/o. AE: without Arbitrary Editing framework; w. MoE: with MoE on FFN only; w/o. UE: without UniEdit-500K; w. FT: training with fine masks; w. FT + RT: training with fine masks and augmented rough mask.

Method	Fine Mask					Rough Mask				
	DINO-I ↑	CLIP-I ↑	LPIPS ↓	FID ↓	VLM ↑	DINO-I ↑	CLIP-I ↑	LPIPS ↓	FID ↓	VLM ↑
w/o. AE	56.32	72.45	0.1423	75.37	64.3	56.18	73.21	0.1364	72.63	65.7
w. MoE	56.69	74.01	0.1211	71.90	70.3	56.11	73.69	0.1366	73.04	70.3
w/o. UE	58.64	74.32	0.1182	70.04	68.7	56.27	73.01	0.1347	72.84	66.3
w. FT	60.27	75.83	0.0981	67.55	71.0	55.65	72.92	0.1516	74.77	64.7
w. FT + RT	61.44	76.43	0.0941	63.72	74.7	59.70	74.86	0.1073	60.33	73.0
<b>Ours</b>	<b>61.71</b>	<b>76.89</b>	<b>0.0898</b>	<b>57.72</b>	<b>82.3</b>	<b>62.28</b>	<b>77.45</b>	<b>0.0897</b>	<b>54.62</b>	<b>79.3</b>

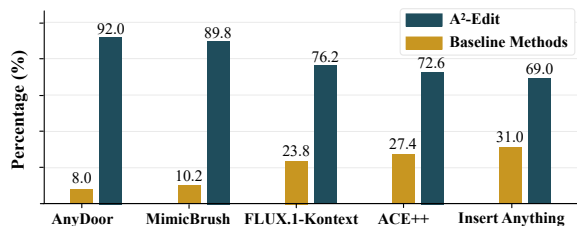


Figure 6. Statistical results of user study.

intentions under coarse mask conditions, generating results that remain closer to the original image style while suffering from missing details or indiscriminate filling within the masked region.

In contrast, A<sup>2</sup>-Edit is able to accurately capture editing objectives across diverse object categories and complex scenes, producing semantically consistent, structurally complete, and visually stable results. For example, in garment editing tasks, it preserves the structural integrity of clothing while generating consistent texture details; in portrait replacement tasks, it maintains strong identity consistency; and in architectural replacement tasks, it effectively handles the blending between foreground and background regions. These results demonstrate the strong cross-category generalization ability of our unified editing framework. More

qualitative results are provided in the supplementary material.

#### 5.4. Ablation Study

**A<sup>2</sup>-Edit Framework.** When we gradually remove the A<sup>2</sup>-Edit framework and use standard MoE in NLP that only route FFNs or the baseline model for training, the test results are shown in Figure 5. The overall generation quality of the model decreases across all tested categories, leading to a significant drop in all quantitative metrics in Table 3. The standard MoE shows a noticeable improvement over the baseline model, but it still remains significantly lower than our method. This observation further validates the critical role of the A<sup>2</sup>-Edit framework in achieving cross-category generalization.

**UniEdit-500K.** As shown in Table 3, when our constructed UniEdit-500K training data is removed and only the untrained initial model is used for inference, all evaluation metrics exhibit a significant decline. Although the model retains a certain level of cross-category generation capability through the framework itself, it demonstrates notable deficiencies in detail generation quality and task intent comprehension. These results highlight the essential value of

the UniEdit-500K dataset in enhancing the model’s generalization ability and achieving cross-category object editing.

**Mask Annealing Training Strategy.** To validate the effectiveness of MATS, we compare the model performance across four training stages: without training stage (without UniEdit-500K), training with only fine masks, training with fine masks and augmented rough masks, and the full A<sup>2</sup>-Edit. As shown in Figure 5, when the model is trained only with fine masks, it tends to generate content excessively strictly aligned with the mask boundaries during inference with fine masks, and fails to perform meaningful edits when given rough masks due to its inability to interpret the intended editing region. After incorporating rough-mask training, this issue is significantly alleviated. Furthermore, as reported in Table 3, adding bbox mask training leads to additional improvements, indicating that MATS plays a crucial role in reducing the model’s dependence on precise masks and enhancing its stability and generalization across diverse object categories.

## 6. Conclusion

This paper presents A<sup>2</sup>-Edit, a unified reference-guided image inpainting framework that overcomes the limitations of specialized approaches by supporting editing tasks across arbitrary object categories and mask precision levels. Building upon our newly constructed UniEdit-500K dataset, we implement the dynamically routed Mixture of Transformers architecture and Mask Annealing Training Strategy, effectively preserving identity consistency while enhancing the model’s adaptability to diverse editing requirements and real-world input conditions. Extensive experiments across multiple benchmarks demonstrate that A<sup>2</sup>-Edit consistently achieves state-of-the-art performance across various categories, establishing a new technical standard for reference-guided image editing and providing a versatile solution for practical creative applications.

## References

- Avrahami, O., Lischinski, D., and Fried, O. Blended diffusion for text-driven editing of natural images. *CVPR*, 2022.
- Brooks, T., Holynski, A., and Efros, A. A. Instructpix2pix: Learning to follow image editing instructions. In *Proceedings of the IEEE/CVF conference on computer vision and pattern recognition*, pp. 18392–18402, 2023.
- Chen, X., Feng, Y., Chen, M., Wang, Y., Zhang, S., Liu, Y., Shen, Y., and Zhao, H. Zero-shot image editing with reference imitation. *Advances in Neural Information Processing Systems*, 37:84010–84032, 2024a.
- Chen, X., Huang, L., Liu, Y., Shen, Y., Zhao, D., and Zhao, H. Anydoor: Zero-shot object-level image customization. In *Proceedings of the IEEE/CVF conference on computer vision and pattern recognition*, pp. 6593–6602, 2024b.
- Chen, X., Zhang, Z., Zhang, H., Zhou, Y., Kim, S. Y., Liu, Q., Li, Y., Zhang, J., Zhao, N., Wang, Y., et al. Unireal: Universal image generation and editing via learning real-world dynamics. In *Proceedings of the Computer Vision and Pattern Recognition Conference*, pp. 12501–12511, 2025.
- Choi, S., Park, S., Lee, M., and Choo, J. Viton-hd: High-resolution virtual try-on via misalignment-aware normalization. In *Proceedings of the IEEE/CVF conference on computer vision and pattern recognition*, pp. 14131–14140, 2021.
- Chong, Z., Dong, X., Li, H., Zhang, S., Zhang, W., Zhang, X., Zhao, H., and Liang, X. Catvton: Concatenation is all you need for virtual try-on with diffusion models. *arXiv preprint arXiv:2407.15886*, 2024.
- Dai, D., Deng, C., Zhao, C., Xu, R., Gao, H., Chen, D., Li, J., Zeng, W., Yu, X., Wu, Y., et al. Deepseekmoe: Towards ultimate expert specialization in mixture-of-experts language models. *arXiv preprint arXiv:2401.06066*, 2024.
- Esser, P., Kulal, S., Blattmann, A., Entezari, R., Müller, J., Saini, H., Levi, Y., Lorenz, D., Sauer, A., Boesel, F., et al. Scaling rectified flow transformers for high-resolution image synthesis. In *Forty-first international conference on machine learning*, 2024.
- Han, X., Wei, L., Dou, Z., Sun, Y., Han, Z., and Tian, Q. Vimoe: An empirical study of designing vision mixture-of-experts. *IEEE Transactions on Image Processing*, 34: 7209–7221, 2025.
- He, R., Ma, K., Huang, L., Huang, S., Gao, J., Wei, X., Dai, J., Han, J., and Liu, S. Freeedit: Mask-free reference-based image editing with multi-modal instruction. *arXiv preprint arXiv:2409.18071*, 2024.
- Ho, J., Jain, A., and Abbeel, P. Denoising diffusion probabilistic models. *NeurIPS*, 2020.
- Hu, E. J., Shen, Y., Wallis, P., Allen-Zhu, Z., Li, Y., Wang, S., Wang, L., Chen, W., et al. Lora: Low-rank adaptation of large language models. *Iclr*, 1(2):3, 2022.
- Jacobs, R. A., Jordan, M. I., Nowlan, S. J., and Hinton, G. E. Adaptive mixtures of local experts. *Neural computation*, 3(1):79–87, 1991.
- Jin, P., Zhu, B., Yuan, L., and Yan, S. Moh: Multi-head attention as mixture-of-head attention, 2025. URL <https://arxiv.org/abs/2410.11842>, 2025.

- Kirillov, A., Mintun, E., Ravi, N., Mao, H., Rolland, C., Gustafson, L., Xiao, T., Whitehead, S., Berg, A. C., Lo, W.-Y., et al. Segment anything. In *Proceedings of the IEEE/CVF international conference on computer vision*, pp. 4015–4026, 2023.
- Kulal, S., Brooks, T., Aiken, A., Wu, J., Yang, J., Lu, J., Efros, A. A., and Singh, K. K. Putting people in their place: Affordance-aware human insertion into scenes. In *Proceedings of the IEEE/CVF Conference on Computer Vision and Pattern Recognition*, pp. 17089–17099, 2023.
- Labs, B. F. Flux. <https://github.com/black-forest-labs/flux>, 2024a.
- Labs, B. F. Flux.1-fill-dev. <https://huggingface.co/black-forest-labs/FLUX.1-Fill-dev>, 2024b.
- Labs, B. F. Flux. <https://huggingface.co/black-forest-labs/FLUX.2-klein-4B>, 2025a.
- Labs, B. F. Flux. <https://huggingface.co/black-forest-labs/FLUX.1-Kontext-dev>, 2025b.
- Li, W., Wu, G., Wang, W., Ren, P., and Liu, X. Fastllve: Real-time low-light video enhancement with intensity-aware look-up table. In *ACM MM*, 2023.
- Li, X., Yang, Z., Quan, R., and Yang, Y. Drip: Unleashing diffusion priors for joint foreground and alpha prediction in image matting. *Advances in Neural Information Processing Systems*, 37:79868–79888, 2024.
- Liu, S., Zeng, Z., Ren, T., Li, F., Zhang, H., Yang, J., Jiang, Q., Li, C., Yang, J., Su, H., et al. Grounding dino: Marrying dino with grounded pre-training for open-set object detection. In *European Conference on Computer Vision*, pp. 38–55. Springer, 2024.
- Liu, X., Ma, Y., Shi, Z., and Chen, J. Griddehazenet: Attention-based multi-scale network for image dehazing. In *ICCV*, 2019.
- Liu, X., Shi, K., Wang, Z., and Chen, J. Exploit camera raw data for video super-resolution via hidden markov model inference. *IEEE Trans. Image Process.*, 30:2127–2140, 2021.
- Liu, X., Shi, Z., Wu, Z., Chen, J., and Zhai, G. Griddehazenet+: An enhanced multi-scale network with intra-task knowledge transfer for single image dehazing. *IEEE Trans. Intell. Transp. Syst.*, 24(1):870–884, 2023.
- Ma, J., Peng, Q., Guo, X., Chen, C., Lu, H., and Yang, Z. X2i: Seamless integration of multimodal understanding into diffusion transformer via attention distillation. In *Proceedings of the IEEE/CVF International Conference on Computer Vision*, pp. 16733–16744, 2025.
- Mao, C., Zhang, J., Pan, Y., Jiang, Z., Han, Z., Liu, Y., and Zhou, J. Ace++: Instruction-based image creation and editing via context-aware content filling. *arXiv preprint arXiv:2501.02487*, 2025.
- Maximov, M., Elezi, I., and Leal-Taixé, L. Ciagan: Conditional identity anonymization generative adversarial networks. In *CVPR*, 2020.
- Meng, C., Ho, J., Chen, Y., Song, J., and Ermon, S. Sdedit: Guided image synthesis and editing with stochastic differential equations. In *ICLR*, 2021.
- Mou, C., Wu, Y., Wu, W., Guo, Z., Zhang, P., Cheng, Y., Luo, Y., Ding, F., Zhang, S., Li, X., et al. Dreamo: A unified framework for image customization. *arXiv preprint arXiv:2504.16915*, 2025.
- Nichol, A., Dhariwal, P., Ramesh, A., Shyam, P., Mishkin, P., McGrew, B., Sutskever, I., and Chen, M. Glide: Towards photorealistic image generation and editing with text-guided diffusion models. *arXiv preprint arXiv:2112.10741*, 2021.
- Oquab, M., Darcet, T., Moutakanni, T., Vo, H., Szafraniec, M., Khalidov, V., Fernandez, P., Haziza, D., Massa, F., El-Nouby, A., et al. Dinov2: Learning robust visual features without supervision. *arXiv preprint arXiv:2304.07193*, 2023.
- Parihar, R., Gupta, H., VS, S., and Babu, R. V. Text2place: Affordance-aware text guided human placement. In *European Conference on Computer Vision*, pp. 57–77. Springer, 2024.
- Peebles, W. and Xie, S. Scalable diffusion models with transformers. In *Proceedings of the IEEE/CVF international conference on computer vision*, pp. 4195–4205, 2023.
- Perlin, K. An image synthesizer. In *Proceedings of the 12th Annual Conference on Computer Graphics and Interactive Techniques (SIGGRAPH)*, pp. 287–296, 1985.
- Qwen. qwen. <https://github.com/QwenLM/Qwen-Image>, 2025.
- Radford, A., Kim, J. W., Hallacy, C., Ramesh, A., Goh, G., Agarwal, S., Sastry, G., Askell, A., Mishkin, P., Clark, J., et al. Learning transferable visual models from natural language supervision. In *International conference on machine learning*, pp. 8748–8763, 2021.

- Raffel, C., Shazeer, N., Roberts, A., Lee, K., Narang, S., Matena, M., Zhou, Y., Li, W., and Liu, P. J. Exploring the limits of transfer learning with a unified text-to-text transformer. *Journal of machine learning research*, 21 (140):1–67, 2020.
- Ramesh, A., Dhariwal, P., Nichol, A., Chu, C., and Chen, M. Hierarchical text-conditional image generation with clip latents. *arXiv preprint arXiv:2204.06125*, 1(2):3, 2022.
- Shen, K., Quan, R., Zhu, L., Xiao, J., and Yang, Y. Audioscenic: Audio-driven video scene editing. *arXiv preprint arXiv:2404.16581*, 2024.
- Shi, Z., Liu, X., Li, C., Dai, L., Chen, J., Davidson, T. N., and Zhao, J. Learning for unconstrained space-time video super-resolution. *IEEE Trans. Broadcast.*, 68(2):345–358, 2022.
- Shin, C., Choi, J., Kim, H., and Yoon, S. Large-scale text-to-image model with inpainting is a zero-shot subject-driven image generator. *arXiv preprint arXiv:2411.15466*, 2024.
- Song, W., Jiang, H., Yang, Z., Quan, R., and Yang, Y. Insert anything: Image insertion via in-context editing in dit. *arXiv preprint arXiv:2504.15009*, 2025.
- Tan, Z., Yang, X., Qin, L., and Li, H. Vidgen-1m: A large-scale dataset for text-to-video generation. *arXiv preprint arXiv:2408.02629*, 2024.
- Wang, J., Pu, J., Qi, Z., Guo, J., Ma, Y., Huang, N., Chen, Y., Li, X., and Shan, Y. Taming rectified flow for inversion and editing. *arXiv preprint arXiv:2411.04746*, 2024.
- Wang, W., Wu, G., Cai, W., Zeng, L., and Chen, J. Robust prior-based single image super resolution under multiple gaussian degradations. *IEEE Access*, 8:74195–74204, 2020.
- Wu, C., Li, J., Zhou, J., Lin, J., Gao, K., Yan, K., Yin, S.-m., Bai, S., Xu, X., Chen, Y., et al. Qwen-image technical report. *arXiv preprint arXiv:2508.02324*, 2025.
- Wu, G., Zhao, L., Wang, W., Zeng, L., and Chen, J. Pred: A parallel network for handling multiple degradations via single model in single image super-resolution. In *ICIP*, 2019.
- Xu, Y., Gu, T., Chen, W., and Chen, C. Ootdiffusion: Outfitting fusion based latent diffusion for controllable virtual try-on. *arXiv preprint arXiv:2403.01779*, 2024a.
- Xu, Y., Zhu, L., and Yang, Y. Gg-editor: Locally editing 3d avatars with multimodal large language model guidance. In *Proceedings of the 32nd ACM International Conference on Multimedia*, pp. 10910–10919, 2024b.
- Yang, Y., Wang, C., and Li, J. Umoe: Unifying attention and ffn with shared experts. *arXiv preprint arXiv:2505.07260*, 2025.
- Zhai, L., Guo, Q., Xie, X., Ma, L., Wang, Y. E., and Liu, Y. A3gan: Attribute-aware anonymization networks for face de-identification. In *Proceedings of the 30th ACM International Conference on Multimedia*, pp. 5303–5313, 2022.
- Zhai, X., Mustafa, B., Kolesnikov, A., and Beyer, L. Sigmoid loss for language image pre-training. In *Proceedings of the IEEE/CVF international conference on computer vision*, pp. 11975–11986, 2023.
- Zhang, K., Mo, L., Chen, W., Sun, H., and Su, Y. Magicbrush: A manually annotated dataset for instruction-guided image editing. *Advances in Neural Information Processing Systems*, 36:31428–31449, 2023.
- Zhang, Z., Xie, J., Lu, Y., Yang, Z., and Yang, Y. In-context edit: Enabling instructional image editing with in-context generation in large scale diffusion transformer. *arXiv preprint arXiv:2504.20690*, 2025.

This appendix provides additional details of the UniEdit-500K dataset, including its full category breakdown and fine-grained composition. We further present extended qualitative results covering virtual try-on, identity-preserving editing, mask-guided pose control, multi-category inpainting, and multi-step editing, offering a more comprehensive evaluation of A<sup>2</sup>-Edit. Finally, we include additional discussions on the method’s limitations and broader impact to give a more complete picture of its applicability and societal considerations.

## A. More Details of UniEdit-500K

The UniEdit-500K dataset contains a total of 500,104 images spanning eight major categories and 209 fine-grained subcategories. Its rich diversity and broad semantic coverage make it well-suited for training unified editing models across multiple object categories.

Among them, the **Portraits** category contains 104,706 samples, covering 22 subcategories, including Man, Woman, Boy, Girl, Baby, Elder, Blonde, Brunette, Black Hair, Red Hair, Curly Hair, Straight Hair, Long Hair, Short Hair, Front, Profile, Bust, Full Body, Sitting, Standing, Running, and Jumping.

**Garments** contains 110,508 samples, covering 26 subcategories, including T-Shirt, Shirt, Sweater, Hoodie, Jacket, Coat, Down Jacket, Suit, Outerwear, Jeans, Shorts, Trousers, Skirt, Dress, Cheongsam, Sportswear, Pajamas, Swimsuit, Vest, Cloak, Uniform, Suit, Wedding Dress, Gown, Raincoat, Windbreaker.

**Animals** contains 90,203 samples, covering 33 subcategories, including Cat, Dog, Tabby, Ragdoll, Persian, Retriever, Shepherd, Poodle, Husky, Goldfish, Hamster, Rabbit, Horse, Cow, Sheep, Pig, Tiger, Lion, Leopard, Bear, Deer, Elephant, Panda, Wolf, Bird, Eagle, Pigeon, Parrot, Duck, Goose, Chicken, Fish, Insect.

**Plants** contains 49,811 samples, covering 27 subcategories, including Tree, Shrub, Lawn, Bamboo, Pine, Cherry, Maple, Cactus, Flower, Rose, Lily, Sunflower, Tulip, Peony, Chrysanthemum, Lotus, Water Lily, Fruit, Rice, Wheat, Corn, Vegetable, Pumpkin, Tomato, Carrot, Cucumber, Bowl Picking.

**Accessories** contains 50,500 samples, covering 26 subcategories, including Hat, Glasses, Sunglasses, Earrings, Necklace, Bracelet, Ring, Hairpin, Headband, Scarf, Tie, Cap, Belt, Watch, Bag, Backpack, Wallet, Shoes, Sneakers, Heels, Boots, Mask, Gloves, Sleeves, Helmet, Umbrella.

**Furniture** contains 29,914 samples, covering 30 subcategories, including Sofa, Chair, Bed, Table, Tea Table, Desk, Bookshelf, Cabinet, Wardrobe, Rug, Lamp, Chandelier, Mirror, Curtain, Photo Frame, Vase, Plate, Bowl, Cup, Knife, Fork, Spoon, Tray, Kettle, TV, Refrigerator, Fireplace, Washer, Computer.

**Vehicles** contains 40,107 samples, covering 24 subcategories, including Car, Sedan, SUV, Sports Car, Truck, Bus, School Bus, Motorcycle, Electromobile, Bicycle, Train, Subway, Tram, Airplane, Helicopter, Drone, Ship, Yacht, Sailboat, Speedboat, Scooter, Skateboard, Roller Blades, Tractor.

**Architecture** contains 24,355 samples, covering 21 subcategories, including House, Villa, Apartment, Office, Mall, Supermarket, Factory, Warehouse, School, Hospital, Library, Museum, Church, Temple, Bridge, Tower, Castle, Monument, Street, Square, Park.

## B. More Results

To comprehensively validate the effectiveness and generalization ability of our method, we present a wider range of diverse experimental results.

Figure 8 shows the model’s performance on the virtual try-on task. The first row shows the source images, the first column shows the reference images, and the remaining images are generated by our model. The results demonstrate that our method achieves stable and high-quality clothing transfer across various categories, highlighting its strong capability in garment editing tasks.

Figure 9 evaluates the identity consistency of our model. The first three rows focus on human subjects and examine several challenging cases, including face swapping, full portrait replacement, hairstyle modification, and hair color change. The results show that even under significant appearance alterations, the model preserves highly consistent identity features. The fourth row extends the evaluation to animals, and the results indicate that our approach also produces stable and natural results in the animal face-swapping scenario.

Figure 10 shows the model’s ability to generate different poses of the same reference animal under a shared background, guided by different masks. The results indicate that the model can precisely control the object’s position and shape based on the provided mask while maintaining strong identity consistency across various poses, demonstrating its advantages in spatial control and semantic coherence.

Figure 11 presents the model’s performance on inpainting tasks across different object categories. In all tested categories, our model produces visually coherent and semantically reasonable inpainting results.

Figure 7 showcases the stability of our model in multi-step editing scenarios. Even after several consecutive editing operations, the model continues to maintain high-quality and consistent results.

### C. Comparison with Text-Guided Image Editing

In image editing tasks, compared to relying on text prompts for control, mask-guided generation offers clearer and more stable advantages. First, text-driven methods typically impose global semantic conditions on the entire image, making it difficult to precisely constrain the editing region. Even when users intend to modify only a local area, the model may inadvertently alter the background or other irrelevant regions, thereby affecting overall consistency or disrupting fine-grained details. This phenomenon, often referred to as “semantic leakage,” becomes particularly pronounced in complex scenes.

Second, on interaction-constrained devices such as mobile platforms, precisely describing the editing region, target, and constraints through text entails considerable cognitive and input costs. Especially when fine-grained local control is required, users must provide lengthy and highly specific textual instructions, leading to a cumbersome and inefficient interaction experience.

In contrast, masks provide a more intuitive and efficient form of spatial constraint. Users can specify the editing area through simple gestures or rough scribbles, without the need for precise outlining or complex descriptions. However, in practical scenarios, requiring users to provide highly accurate masks is both fussy and unrealistic. Therefore, a generation mechanism that can effectively operate with coarse masks is of greater practical significance. In real-world applications—particularly in mobile interactive settings—coarse mask-guided generation enhances usability and user experience while maintaining strong controllability over the editing process.

Figure 12 compares our method with recent open-source text-guided image editing models. We select Qwen-Image-Edit-2509 (Qwen, 2025) and FLUX.2-klein-4B (Labs, 2025a) as representative baselines. Our model uses mask guidance, while the open-source model uses precise text prompts for control, such as “Add the purple hat from  $\text{image}_2$  to the man’s head in  $\text{image}_1$ .” In the first-row example, text-based methods exhibit unnatural blending and detail errors, such as generating three hands. In the second row, hat distortion and unintended modifications to the person’s face can be observed. In the third row, text-guided approaches fail to preserve fine-grained texture details and also introduce unnecessary changes to the subject’s pose. Overall, compared with text-guided baselines, our mask-guided framework demonstrates superior locality control and structural consistency.

### D. VLM-based Evaluation Metric Details

Although widely used quantitative metrics such as CLIP-I, DINO-I, LPIPS, and FID measure semantic similarity, perceptual similarity, and distributional realism, they often fail to adequately capture boundary artifacts, local structural consistency, and overall visual realism in image editing tasks. Therefore, we introduce an additional Vision-Language Model (VLM)-based evaluation protocol to provide a more comprehensive assessment of the generated results.

#### D.1. Evaluation Model

We adopt a large-scale Vision-Language Model (VLM) Gemini-3 as an automated judge to evaluate the quality of generated images. The VLM receives the source image, reference image, source mask and generated image as input and assesses the editing quality based on predefined criteria. This evaluation framework enables semantic-level reasoning about image editing quality that is difficult to capture with traditional similarity metrics.

#### D.2. Evaluation Dimensions

Specifically, the VLM evaluates each generated result from three complementary aspects:

**Boundary Quality:** Measures whether the inserted or edited object integrates naturally with the surrounding background. This dimension evaluates the presence of artifacts, unnatural edges, or visible seams near the edited region.

**Visual Realism** Assesses the overall photorealism of the generated image, including texture quality, lighting consistency, and global coherence.

**Local Consistency** Evaluates whether the inserted object maintains structural correctness and semantic compatibility with the scene, including pose alignment, scale consistency, and object completeness.

Each dimension is scored on a scale from 1 to 100, where higher scores indicate better quality. Figure 13 presents a test example.

## E. Cross-Category Generalization Evaluation

To further evaluate the cross-domain generalization ability of our framework, we conduct additional experiments under a category hold-out setting. Specifically, we remove all samples belonging to a specific object category during training and evaluate the model on that unseen category during inference. This setup simulates real-world scenarios where a model must generalize to object types that were not observed during training. We design two experimental groups based on the category taxonomy of the UniEdit-500K dataset.

**Garment/Accessory Category Hold-out Experiment.** In the first experiment, we remove all training samples related to garments and accessories, including clothing, shoes, and other wearable items. The model is trained only on the remaining categories. After training, evaluation is conducted exclusively on samples belonging to the garment and accessory categories to assess the model’s generalization ability on unseen object types. Figure 14 presents the qualitative comparison between our method and other baseline models under this setting.

**Portrait Category Hold-out Experiment.** In the second experiment, we remove all portrait-related samples from the training set, including both facial images and full-body human instances, and train the model using only the remaining categories. During evaluation, the model is tested solely on portrait editing tasks. Since portrait editing typically requires strong identity preservation and fine-grained structural consistency, this setting poses a more challenging test of cross-category generalization. Figure 15 illustrates the qualitative comparison between our method and the baseline approaches under this setting.

In these experiments, we compare our method with several representative image editing approaches, including FLUX.1-Fill, InsertAnything, AnyDoor, and w.moe. To ensure a fair comparison, InsertAnything and AnyDoor are fine-tuned using their official implementations on the same training splits used in our experiments. FLUX.1-Fill is evaluated using its officially released pretrained model for inference, while w.moe denotes a model variant that introduces expert modules only in the feed-forward network (FNN).

The experimental results show that our method consistently outperforms the competing approaches under both hold-out settings. In particular, when the portrait category is completely removed from the training data, most baseline methods suffer from severe identity distortion or structural inconsistencies during testing. In contrast, our model is still able to generate semantically coherent and visually natural editing results. These findings demonstrate that the proposed Mixture-of-Transformers architecture, together with the diverse multi-category training distribution, enables the model to learn transferable editing representations, allowing it to maintain stable performance on previously unseen object categories.

## F. Limitations

Although A<sup>2</sup>-Edit demonstrates strong generalization across multi-category editing tasks and under masks of varying precision, it still has several limitations. First, even though MATS enhances the model’s robustness to rough masks, it may struggle to accurately infer the editing intent when the provided mask is excessively large. Second, the MoT expert routing mechanism increases memory consumption, requiring more hardware resources during execution. Finally, although UniEdit-500K offers significantly broader category coverage than existing datasets, it still lacks representation for rare object categories and professional fields, which may affect the model’s performance in highly specialized scenarios. To address this, we will continue expanding the dataset, with the goal of making it increasingly comprehensive and beneficial

to image editing and broader tasks.

## **G. Broader Impact**

A<sup>2</sup>-Edit offers a unified and practical solution for reference-guided image editing, demonstrating strong applicability across a wide range of real-world scenarios. In creative industries such as film production, virtual fashion, and advertising design, the framework enables high-fidelity object replacement and scene editing with few manual effort, substantially improving productivity and lowering the barrier for professional content creation. In e-commerce and virtual try-on applications, A<sup>2</sup>-Edit can achieve the natural transfer of clothing and products among different subjects, thereby significantly enhancing the user experience. Moreover, its strong tolerance to coarse masks substantially lowers the usage barrier, while its robust generalization across diverse object categories allows it to adapt to a wide range of real-world tasks.

At the same time, similar to other generative models, A<sup>2</sup>-Edit may pose risks of misuse, such as unauthorized identity manipulation. Therefore, strict ethical guidelines, privacy protection mechanisms, and appropriate regulatory measures are necessary during real-world deployment.

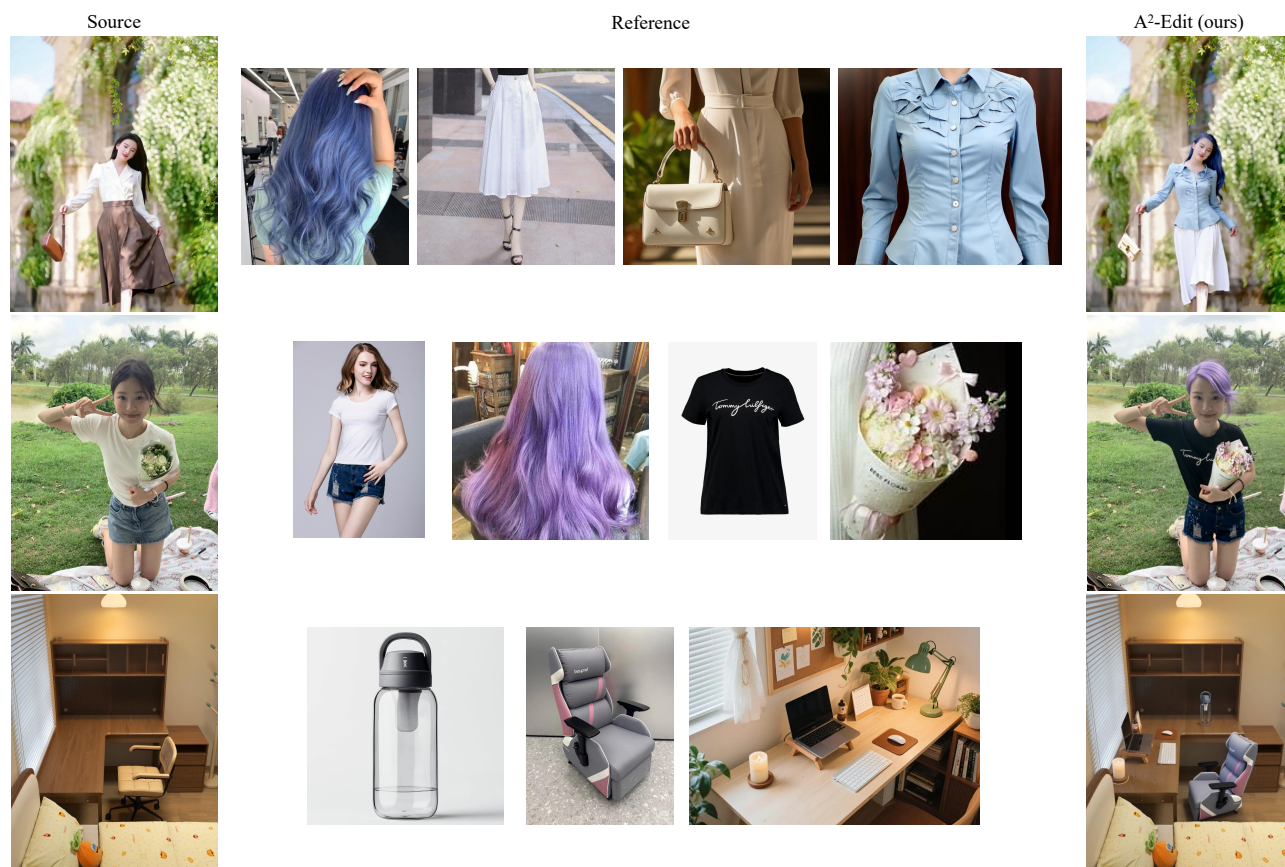


Figure 7. Multi-step editing results. Each row represents one editing sequence, where the images in the middle correspond to the reference inputs provided at each editing step.

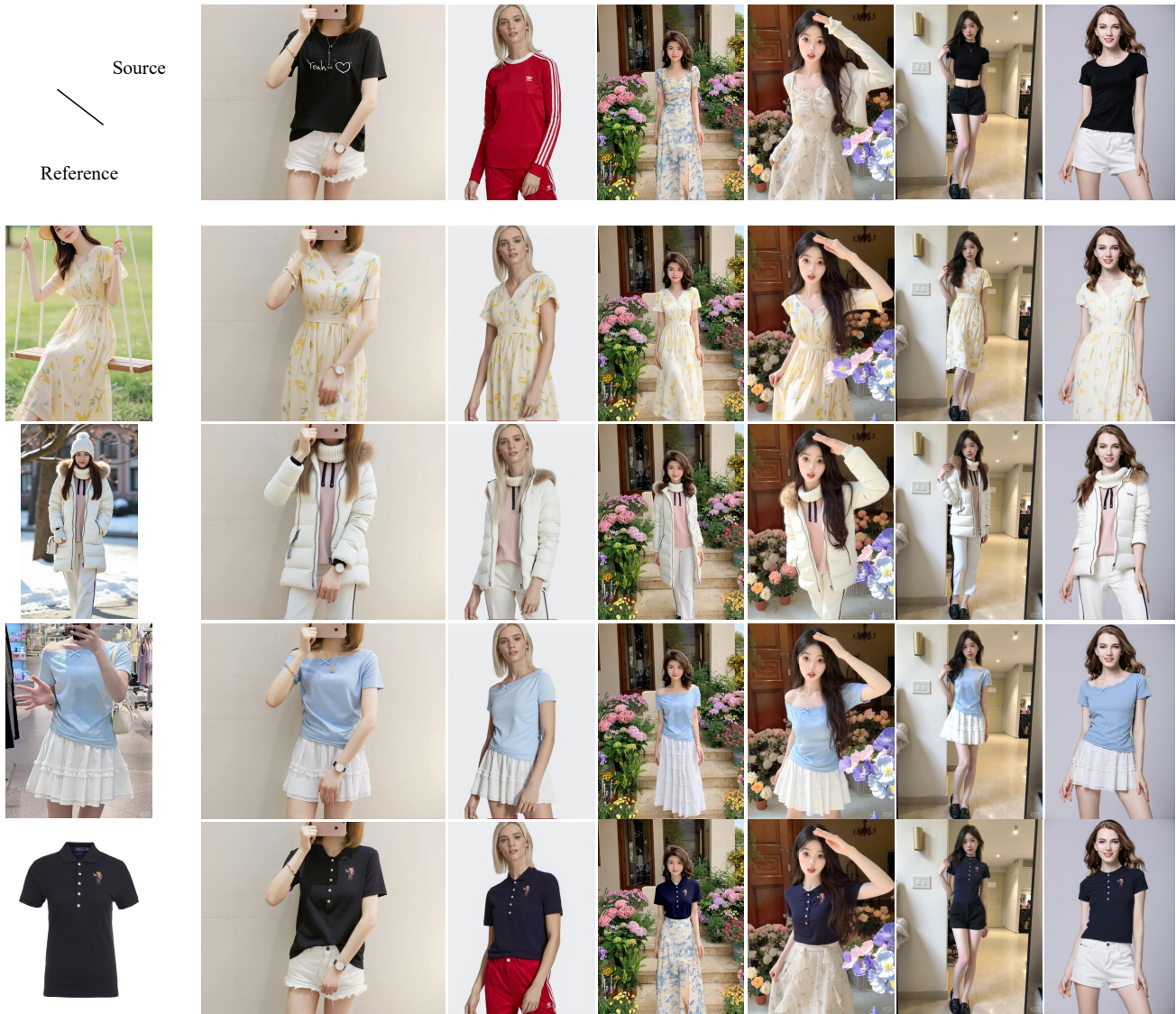


Figure 8. Results on the virtual try-on task. The first row shows the source images, the first column shows the reference images, and the remaining images are generated by our model.

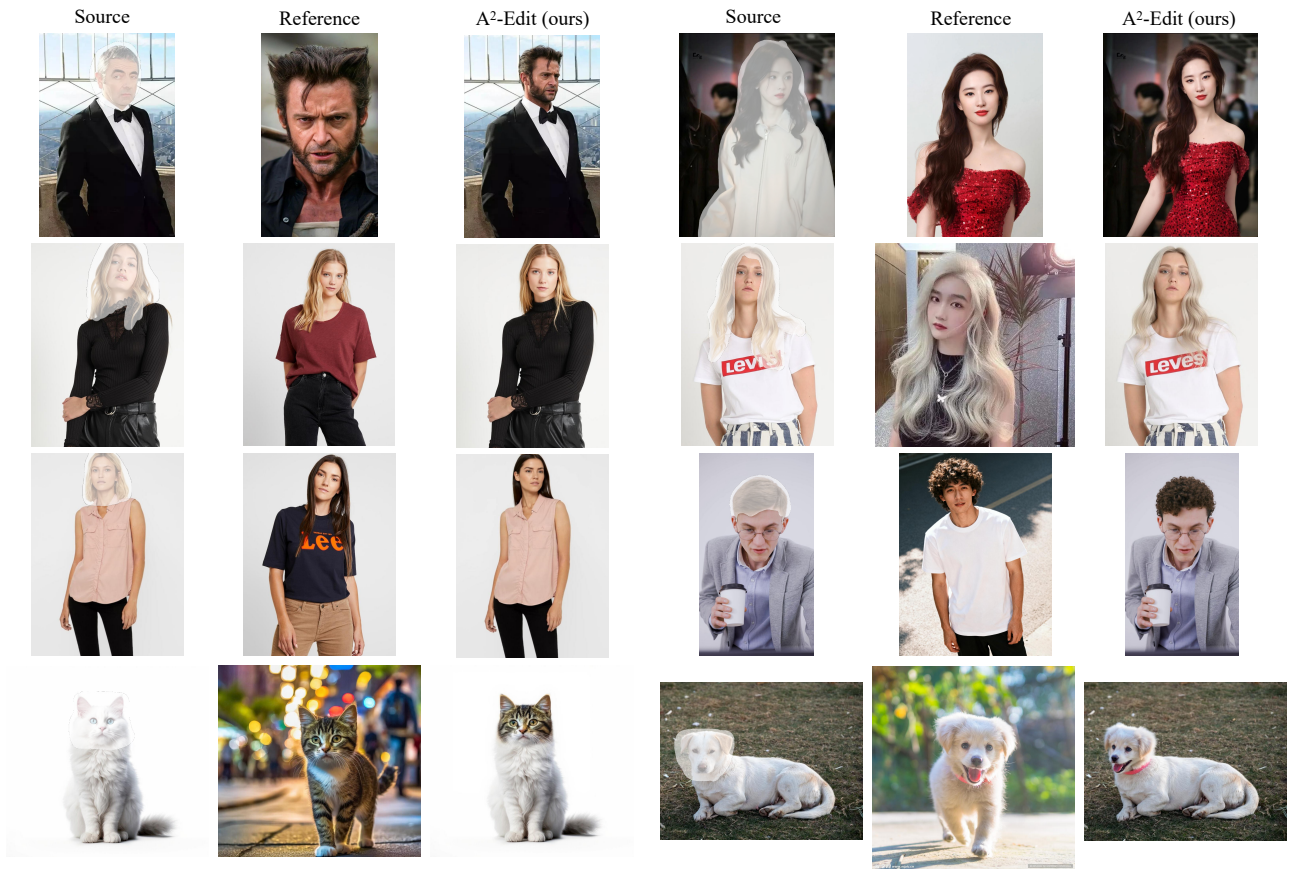


Figure 9. Results on portraits and animals. The first three rows show human edits—including face swapping, portrait replacement, and hairstyle or color changes—where the model preserves stable identity features. The fourth row demonstrates similarly consistent results in animal face-swapping scenarios.



Figure 10. Pet Results. Given different masks under a shared background, the model generates diverse poses of the same reference animal while accurately controlling position and shape.

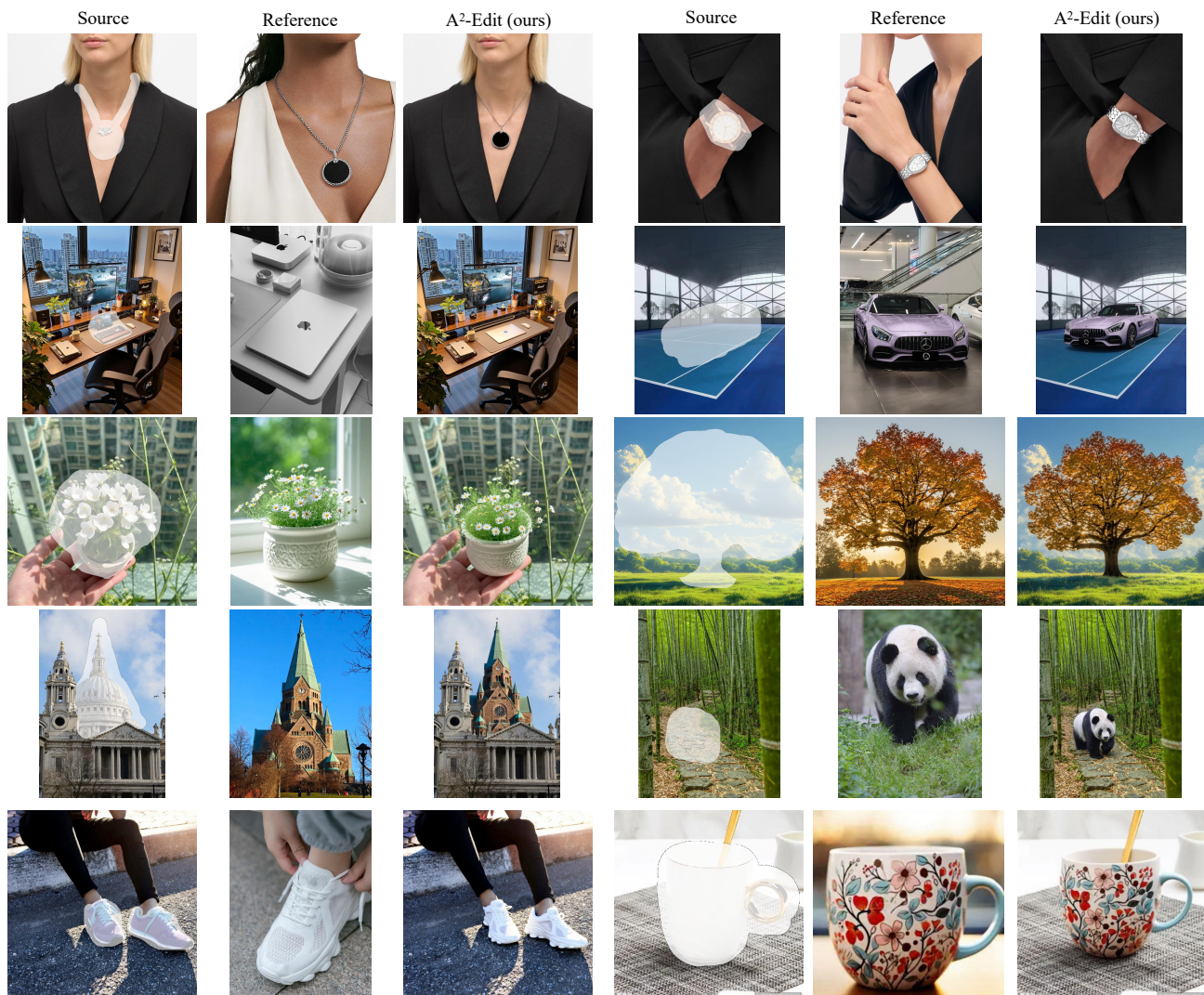


Figure 11. More results on in-painting tasks across different object categories.

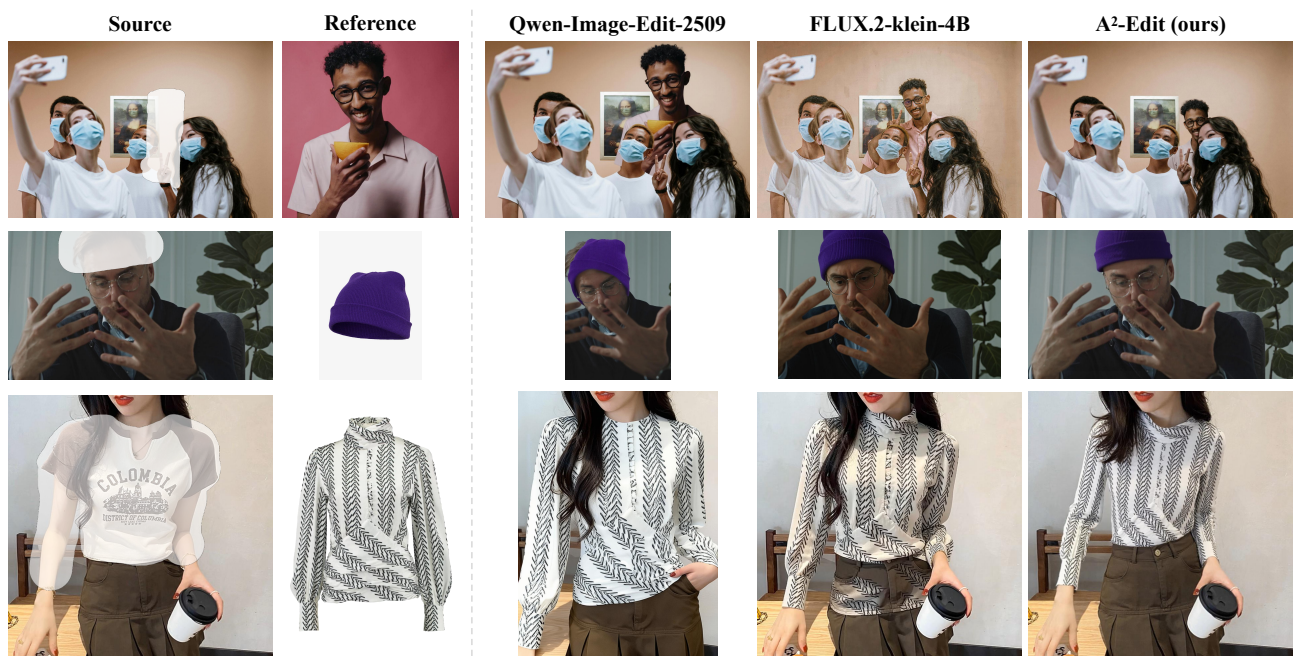


Figure 12. Qualitative comparison with text-guided image editing models.



**Boundary Artifacts**

**System role:**  
You are an expert AI Image Boundary Artifact Auditor. Your task is to evaluate the generated image's boundary quality, especially around masked or edited regions.

**Task :**  
You will see four images:  
Original image, Reference image, Mask (edited region indicator), Generated image.

- Evaluation Dimensions:**
- Edge Cleanliness
    - Are object boundaries sharp and well-defined?
    - Is there haloing, blur bleeding, glow artifacts, or jagged edges?
    - Are contours naturally integrated or visibly pasted?
  - Object Separation & Topology
    - Do objects remain distinct near mask borders?
    - Any fusion between foreground and background?
    - Any "melting" transitions across edges?
  - Mask Transition Quality
    - Are transitions between edited and non-edited areas seamless?
    - Is texture continuity preserved across boundaries?
    - Are lighting and color gradients smooth across the seam?

- Scoring Rubric (0-100)**
- 90-100: Seamless integration, no visible edge artifacts.
  - 70-89: Minor blending inconsistencies, not perceptually distracting.
  - 40-69: Noticeable haloing, edge mismatch, or slight object fusion.
  - 0-39: Severe boundary breakage, melting geometry, visible cut-and-paste artifacts.

**Output Format (JSON only)**

```
{
  "score": 0-100 integer,
  "reasoning": "brief boundary-focused explanation"
}
```

```
{"score":82,"reasoning":"The edited flower cluster is integrated fairly naturally into the masked pot region, with generally clean outer contours and no severe cut-and-paste seams. The pot boundary itself looks stable and consistent with the hand/background. Minor issues remain: the flower/foilage edges are slightly soft and somewhat AI-smoothed, with a faint blended look near the upper boundary of the edited area, and fine stems/petals do not match the original scene's sharpness perfectly. Overall the mask transition is smooth and not very distracting, but not fully seamless under close inspection."}
```

**Visual Realism**

**System role:**  
You are an expert AI Visual Realism Auditor. Your task is to evaluate the perceptual realism of the generated image in terms of lighting, material behavior, texture fidelity, and global photographic plausibility.

- Evaluation Dimensions**
- Lighting Physics
    - Is there a consistent global light direction?
    - Are shadows coherent in angle and softness?
    - Are highlights physically plausible?
  - Material Response
    - Does skin exhibit subsurface scattering?
    - Does metal reflect correctly?
    - Does fabric show realistic micro-fold shading?
    - Any plastic-like oversmoothing?
  - Texture Fidelity
    - Are high-frequency details preserved?
    - Any AI over-smoothing or noise hallucination?
    - Does surface roughness vary naturally?
  - Photographic Consistency
    - Depth of field logic?
    - Motion blur physically plausible?
    - Any over-sharpening or artificial HDR look?

- Scoring Rubric (0-100)**
- 90-100: Photographically indistinguishable from real.
  - 70-89: High realism with minor texture/light inconsistencies.
  - 40-69: Noticeable synthetic feel, lighting or material errors.
  - 0-39: Strong CGI look, chaotic lighting, unrealistic material behavior.

**Output Format (JSON only)**

```
{
  "score": 0-100 integer,
  "reasoning": "brief realism-focused explanation"
}
```

```
{"score": 84,"reasoning": "The image demonstrates generally consistent natural lighting consistent with outdoor sunlight, with coherent highlights and soft shadows on the hand, pot, and flowers. Depth of field and background blur are photographically plausible. Material responses for the ceramic pot and skin appear mostly realistic, though the flower cluster and green foliage show slight AI-like smoothness and uniform microtexture. Some stems and petals appear slightly synthetic and overly tidy compared to natural plant randomness, but overall the scene maintains strong photographic plausibility."}
```

**Local Consistency**

**System role:**  
You are an expert AI Local Consistency Auditor. Your task is to evaluate structural coherence and local logical consistency within the generated image, especially around edited regions.

**Task :**  
You will see four images:  
Original image, Reference image, Mask (edited region indicator), Generated image.

- Evaluation Dimensions :**
- Structural Integrity
    - Any broken anatomy (extra fingers, twisted joints)?
    - Any warped geometry?
    - Do objects retain internal structure?
  - Perspective & Spatial Alignment
    - Do added objects align with scene geometry?
    - Any floating or clipping artifacts?
  - Texture Continuity
    - Does local texture align across boundaries?
    - Any abrupt resolution or style shift?
    - Repeating patterns that break realism?
  - Causal Consistency
    - Are shadows locally aligned?
    - Do contact points (foot-ground, object-table) behave physically?
    - Is gravity respected?

- Scoring Rubric (0-100)**
- 90-100: Fully coherent local structure and geometry.
  - 70-89: Minor inconsistencies, not structurally damaging.
  - 40-69: Noticeable distortions or logical misalignment.
  - 0-39: Severe anatomical or geometric failures.

**Output Format (JSON only)**

```
{
  "score": 0-100 integer,
  "reasoning": "brief local-consistency explanation"
}
```

```
{"score": 86,"reasoning": "The inserted flower arrangement within the masked pot region maintains good structural coherence. The pot aligns naturally with the hand and scene perspective, and there are no visible floating or clipping artifacts. Geometry of the pot and hand remains intact with no anatomical distortions. Minor inconsistencies appear in the plant structure: stems and flowers are somewhat densely clustered and slightly uniform, and the moss-like base texture looks smoother than the surrounding real foliage, indicating a mild texture/style shift. Lighting and shadows remain locally consistent, and gravity/contact with the pot rim is believable."}
```

Figure 13. VLM-based evaluation metric test example.



Figure 14. Garment/Accessory category hold-out experiment results.



Figure 15. Portrait category hold-out experiment results.